Proc Indian Natn Sci Acad **79** No. 4 December 2013 Spl. Issue, Part A, pp. 639-650

DOI: 10.16943/ptinsa/2013/v79i4/47991

Research Paper

Computational Simulation of Fully Deformable Motorcycle Wire-Spoke Wheel

K S TAN[1,2,3], S V WONG[1,2,4*], M M H MEGAT AHMAD[3], R S RADIN UMAR[2] and N KGUPTA[5**]
[1]*Department of Mechanical and Manufacturing Engineering, Faculty of Engineering, Universiti Putra Malaysia, 43400 UPM Serdang, Selangor, Malaysia*
[2]*Road Safety Research Centre, Universiti Putra Malaysia, 43400 UPM Serdang, Selangor, Malaysia*
[3]*Department of Mechanical Engineering, Faculty of Engineering, Universiti Pertahanan Nasional Malaysia, Sungai Besi Camp, 57000 Kuala Lumpur, Malaysia*
[4]*Malaysian Institute of Road Safety Research, 43000 Kajang, Selangor, Malaysia*
[5]*Department of Applied Mechanics, Indian Institute of Technology Delhi, New Delhi 110 016, India*

(Received 20 February 2013; Accepted 08 March 2013)

In motorcycle frontal collision with other vehicles or structures such as roadside objects, front wheel is the component that receives first direct impact. In such a crash, contact reactions between wheel and impacted object influence significantly the subsequent motion of the motorcycle and the rider. Fidelity of the finite element (FE) model of a frontal wheel is thus a crucial factor for accurate and realistic simulations of motorcycle crashes. This paper presents a FE model of a complete wheel-tyre assembly with capability of handling a fully deformable wheel. The wheel considered is a steel rim with wire spokes, used widely in light motorcycles. Major components namely the tyre, inner tube, rim, spokes, hub, hub cover, axle and axle bushing were included in the model and their modelling aspects are discussed in detail. Relevant critical factors ensuring numerical stability and robustness of the model have been identified and discussed. Data from an experimental study on response of the wheel subjected to different impact configurations were used for the validation. This was done by simulating the actual impact experiments and then comparing the results with overall deformation pattern of the wheel, maximum residual crush of the rim, time histories of displacement and velocity of the striker throughout the impact process. The modelling work has been found to successfully reproduce physical response of the wheel in terms of these three key validation indicators and it is concluded that a satisfactory wheel model has been developed.

Key Words: Motorcycle; Wire-Spoke Wheel; Finite Element Modelling; Impact Simulation; Fully Deformable; Motorcycle Crash; Motorcycle Crashworthiness

Introduction

Frontal collision of motorcycle represents the severest type of road crash mechanism whereby the rider is often ejected from the motorcycle and thrown towards the opponent vehicle, striking head-on with the vehicle structure, experiencing serious or fatal head injuries [1, 2]. In such crashes, front wheel is always first and directly contacted part of the motorcycle and the contact impact mechanism mainly affects subsequent motion of both the rider and the motorcycle. Studies suggest that even a small difference such as whether the front tyre of a motorcycle directly hits the centre pillar of a car could yield large differences in its subsequent motion [3]. By implication, fidelity of the model of a motorcycle front wheel is a factor that greatly influences the quality of simulation of motorcycle crashes.

*Author for Correspondence: E-mail: wongsv@miros.gov.my
**Present Address: Supercomputer Education & Research Centre, Indian Institute of Science, Bangalore 560 012, India

A great deal of work has been done in the motorcycle crash simulations since 1970 but the focus on the modelling of its wheel-tyre assembly is still lacking. Incorporation of the spring-damper elements in wheel modelling in [4] provided a more realistic representation as compared to total rigid models. An MB-FE model with moderate details of FE models for the wheel, tyre, fork stem and triple clamp was published in [5]. Full crash simulations with FE oriented model were seen in [6-9], which incorporated a shell elements tyre modelled according to the Takatori's methodology [10] and brick elements for cast rim. But some details of the modelling aspects were missing. Other FE models were also developed as in [11, 12], but without much focus on the wheel part. For the tyre alone, detailed development of the FE model can be traced back to [13], where a bias-ply tyre was modelled using 3-D solid and truss elements. A comprehensive FE model of an aluminium rim with tubeless tyre containing rubber, nylon cord and air, has been purposed for estimating the reaction force of the tyre during impact. However, details considered are too fine for it to be implemented in a typical full crash simulation [3]. In another study [14], two tyres composed of shell and solid elements respectively were developed and design of experimental approach was employed to investigate the material characteristics of tread and sidewall.

In this paper, FE model to simulate a fully deformable wire-spoke wheel using LS-DYNA explicit solver [16] is presented. The modelling work reproduces the impact tests [15] well. Important considerations in regard to these tests, details of the model development and finally the validation aspects are discussed.

The Experimental Work

The experimental work in [15] consists of a series of impact tests performed on the motorcycle steel rim wire-spoke wheel under various configurations using factorial design approach. The study provides significant useful data for investigating the impact behaviour of the wheel and therefore has been used in the present study for the validation purpose. The experiments also give useful insights in establishing the scope of the modelling work.

Generally, in computational simulations, as the impact conditions and deformations become severe, chances of getting numerical instabilities increase. In other words, a model that is capable of simulating complex conditions would be capable of handling less complex ones too, but not the other way. Hence to ensure a sufficiently stable and robust model, configuration that serves as the reference for initial simulation needs to be selected from those with impact load based on maximum residual crush, δ, defined as residual radial displacement of the outermost deformed edge of the rim, shown in Fig. 1. Based on the values of δ, severity of deformation can be classified into four groups: 4^{+1}_{-1} mm; 28^{+12}_{-12} mm; 78^{+15}_{-17} mm; 141^{+17}_{-20} mm. These groups correspond to the dissipated impact energy levels of approximately 100-150 J, 300-340 J, 730-820 J and 1570-1710 J, respectively [15]. For the energy levels up to 820 J, the hubs were generally intact with only insignificant and localized deformation in the region of holes where spokes were hooked on. But hubs mostly sustained catastrophic failure under higher impact loads of the group four [17]. Moreover, some offset impacts tend to cause catastrophic failure even at moderate impact intensity. In the present study, such cases have not been considered as certain failure criteria are required and these will be explored after the initial models have been successfully validated. Therefore, the events selected for simulations were those of central impact from the second and third groups. Possible values of various experimental factors and the ones actually considered in different experiments for simulations are given in Tables 1 and 2 respectively. Each configuration is denoted by a letter or combination of letters, in accordance with

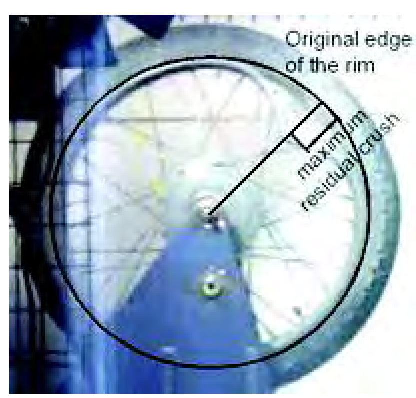

Fig. 1: Definition of residual maximum crush, δ

Table 1: Factorial levels of each factor for the wheel impact test

Factor	Notation	Low (-)	High (+)
Impact speed (ms^{-1})	*S*	3	6
Impact mass (kg)	*M*	51	101
Tyre pressure (kPa)	*P*	148	252
Striker contact geometry measured as nose radius (mm)	*G*	30	100
Vertical impact offset distance from axle (mm)	*D*	0	108

Table 2: Impact configurations for simulations

	1	2	3	4	5	6
Impact configuration	*s*	*m*	*p*	*g*	*spg*	*mpg*

the common notation used in design of experiments. Presence of the particular letter(s) indicates that the level of the corresponding factor(s) is high, else it is low. For example, for the configuration number 12, *spg*, the impact test is run with *S*-high (6 ms^{-1}), *M*-low (51 kg), *P*- high (252 kPa), *G*-high (100 mm) and *D*-low (0, or no offset). Different nose shapes of strikers are shown in Fig. 2.

FE Modelling of Wheel-Tyre Assembly

Rim

The specimen wheel for the impact tests is of the type used extensively in most light motorcycles with engine capacity usually ranging from 75-125 cc, and a dry mass of approximately 100 kg. The wheel

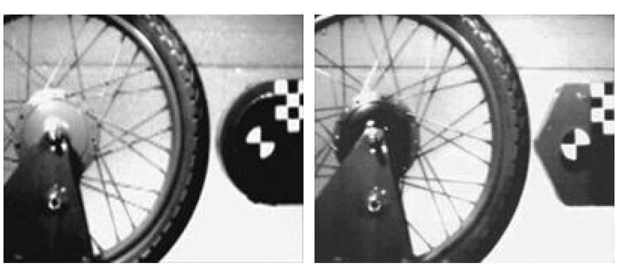

(a) (b)

Fig. 2: Wheel impact test with strikers: (a) cylindrical and (b) triangular

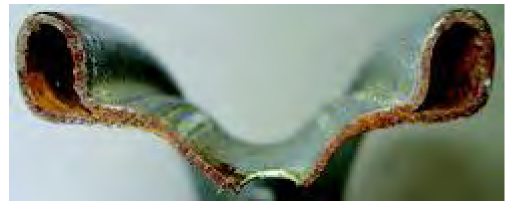

Fig. 3: Cutaway view of a physical rim

(a)

(b)

Fig. 4: (a) Actual arrangement at the hole; (b) simplification in modelling

consists of a 36-spoke steel rim of 17 inches (431.8 mm) diameter with the thickness of 1.40 mm and commonly notated as size 1.40 x 17. The major components of the wheel namely the rim, wire spokes, hub, axle, tyre and rubber tube are included in the model. The rim is WM type with cylindrical bead seat [18], Fig. 3. For its relatively thin cross section, the thin shell elements have been the choice for meshing. The mid surface of the rim was used as the reference geometry for meshing in order to account for the contact thickness to avoid initial penetration in the contact treatment in LS-DYNA environment [16]. Physically the holes for spoke nipples to anchor on are not punched directly on the general surface of the rim but slightly dented to serve as a seat. This feature was simplified in the model as illustrated in Fig. 4.

The rim being of complicated shape, a tensile test for determining its material properties on a specimen extracted from it seemed impractical. Manufacturers would also not share this information for their own reasons. The material input required in this work was therefore estimated based on relevant industrial standards and proper quasi-static compression testing of the whole rim up to its collapse. The rim is typically fabricated from a steel strip of commercial quality (SPCC) [19], and a typical stress-strain (σ-ε) curve of SPCC under quasi-static test (0.03 s-1 strain rate) is available from literature [20]. This curve served as a base σ-ε curve and a simplified version with some data points removed in linear portions was used as a material data of the rim in a compression simulation of the setup as in the experiment. Response of the rim in terms of force versus displacement was used as a reference with which results from equivalent simulation can be compared. Any significant deviation of the simulation results from the experimental data is reflected in the force-displacement curve which signifies the unmatched material properties. It was found that the base σ-ε curve of SPCC yielded relatively low reaction forces in the simulation. Modifications of the curve were then performed by first scaling the base σ-ε curve to retain its general pattern, followed by some fine adjustments of the initial yielding portions. The resulting force-displacement curve from the simulation after several modification attempts is presented in Fig. 5, together with the response from the experiment and the one using the SPCC original material data. The condition of the rim at the end of the test is illustrated in Fig. 6. Close matching of the simulation outcomes with the experiments indicates that the material property of the rim was reasonably estimated. The material model is MAT_PIECEWISE_LINEAR_PLASTICITY. To account for the dynamic loading characteristics, typical values of the strain rate parameters C and P [16] for steel were taken as 40.4 s^{-1} and 5.0, respectively.

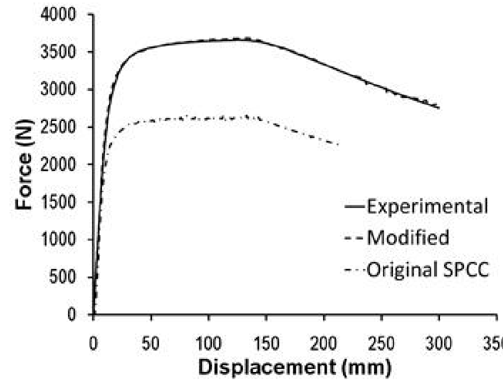

Fig. 5: Comparison of responses of the rim under compression test in terms of force-displacement curves obtained from experiment and simulation

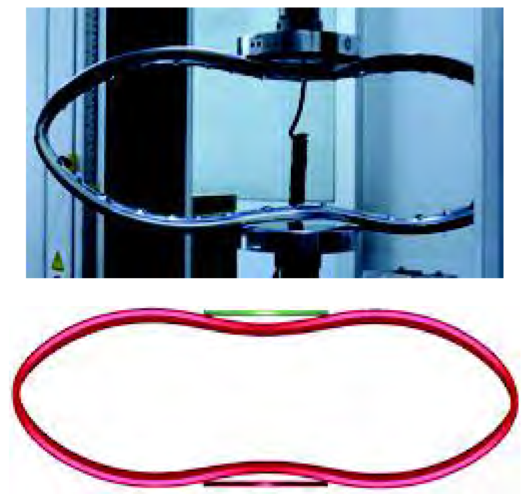

Fig. 6: Deformation of the rim at the end of the compression test

Wire Spokes

When the wheel was subjected to radial compression, the rim tended to deform into an oval shape. The deformation mechanism progressively increases the tensile force in spokes that are in the major axis of the oval. For a sufficiently high load, the localized deformation at the corresponding hole area would become too severe that can no longer support the tension and the nipple slips off from the rim. Such slip-off behaviour is important in quantifying and characterizing the overall deformation of the wheel. This is due to the fact that during the impact, once the spokes are released from the rim, a larger deformation would be produced, as opposed to the condition of restricted deformation without slip-off. To develop a model with the capability to simulate such phenomenon, some detailing is required. The solid elements were used to mesh the whole spoke instead of simpler beam elements. The gap between the nipple and the hole is very small and thus required relatively fine mesh to preserve the circular shape of the hole in order to prevent initial penetrations.

The spoke pretension can be effectively simulated in a dynamic relaxation phase. The spoke length was slightly reduced from its initial free length at the first stage. Then, in order to place the nipple back on the rim, the spoke was lengthened to a sufficient length by applying nodal load on all the nodes at the dome portion of the nipple. To avoid being misinterpreted as initiation penetration by the solver, the associated contact definition is only invoked when the nipple is fully passed through the hole. At the same time, the loads were totally removed and the nipple will be settling down in the hole, and the preload is introduced at the end of the dynamic relaxation phase. The amount of initial reduction in the spoke length was chosen carefully so that the lengthening process of the spoke to the desired length occurred only in the elastic region for it to have an effective retraction upon load removal.

The material data for the spoke was obtained from uniaxial tensile tests and the corresponding σ-ε curve, simplified as discussed above, is used as the input. The selected material models as well as strain rate parameters are the same as those for the rim.

Hub

While the nipple-end is anchored to the rim at its hook-shape end, the spoke is anchored through a hole on the hub. The hub comprised of mainly the hexahedral elements and some wedge elements at certain locations due to geometrical constraints. The hub model was simplified by ignoring the steel bearing at its centre axle hole and considering the space fully filled up with the hub material. The hub is known to be made of aluminium die-casting alloy, in accordance with the industrial standard JIS H5302 ADC12 or ANSI 383 [22]. But since it shows no significant deformation for the impact configurations concerned, it was modelled as a rigid material with typical properties of aluminium alloy. The aluminium hub cover and steel bushing also show no appreciable deformation so they were also modelled as rigid parts for computational efficiency.

Tyre and Inner Tube

Air pressure in the rubber tube was modelled by defining a pressurized control volume, referred to as an airbag, using the keyword *AIRBAG_SIMPLE_PRESSURE_VOLUME. In the context of the impact test, the main function of the tyre would be simply a cushioning unit that receive and transmit the impact load, but not rotating and bumping on the road where its traction characteristics become relatively crucial. Therefore, cross sectional details are neglected and only the average thicknesses are captured for the respective crown and the sidewall region, so that the final tyre model was composed of distinctive sidewall and tread parts.

The material property of the rubber tube was also determined by a typical uniaxial tensile testing and the force-displacement curve obtained was used as input. Since the tube is contained in the tyre, its deformation would be relatively small under inflation and also throughout the impact. The average elongation is about 29 mm, or a strain of about 21%, which is relatively small for rubber material. The tube can be adequately modelled with the material model MAT_MOONEY-RIVLIN_ RUBBER. The tyre was also modelled by the same material model, and the required values of the corresponding material parameters were obtained from [14].

Bead Wires

At the respective extreme ends of the tyre are steel bead wires which provide the required stiffness to lock the tyre on the rim. The beads must not be neglected in the model to avoid the tyre slip off from the flange as the air pressure builds up. Physically the beads are composed of strands of six individual wires of 1 mm diameter and arranged as shown in Fig. 7a. In the model, each strand is represented by a Belytschko-Schwer resultant beam [21] with equivalent area properties. Nodes were merged between the beam elements and the shell elements of the tyre so they were essentially glued to each other. The resultant beam required the specification of a cross sectional area, a shear area, and area moments of inertia, I_{ss}, I_{tt} and I_{rr} along *s-s*, *t-t* and *r-r* axis, respectively, Fig. 7b. The calculated values for

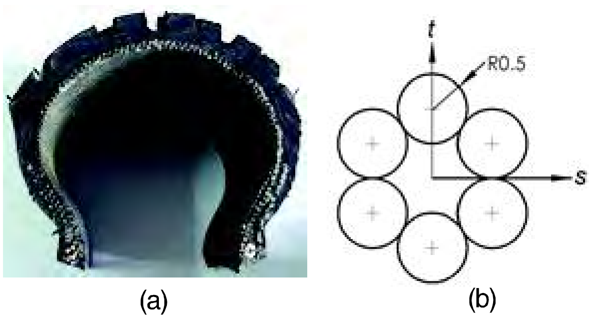

Fig. 7: (a) Encased bead wires in the tyre and (b) cross section of bead wire

the cross sectional area is 4.7124 mm^2, shear area is 4.2412 mm^2, $I_{ss} = I_{tt}$ are 2.6507 mm^4, and I_{rr} is 5.3014 mm^4.The material of the bead wire was modelled by an elastic material, MAT_ELASTIC with typical steel properties.

Axle

The axle experienced significant deflection in the impact tests. For simplification it was modelled as a double-headed bolt to replace the nut end. The hub cover and bushing, although showed no significant deformation in the impact tests, are included to ensure a proper boundary condition and are modelled as rigid parts. No simplification was attempted on the original geometry of the hub cover and the meshing was done via the automatic tetrahedral meshing with relatively small element size in order to maintain the smoothness of the surface of the centre slot having contact with the axle to avoid penetrations. Its material data was obtained from uniaxial tensile tests and the corresponding σ-ε curves are used as the input. The selected material model is MAT_PIECEWISE_ LINEAR_PLASTICITY, same as for the rim and with the same values of the strain rate parameters.

Contact Treatments

The contact treatments for the present modelling were complicated by the presence of rubber tube, due to its relatively low thickness ranging from 1.2 to 1.5 mm and extremely low elastic modulus. The inner tube rubber has the stiffness of only 0.89 MPa (for the strain below 10% and fitted linearly), which is 22470 times smaller than that of 200 GPa of the steel rim and spoke. The geometrical nonlinearity of the rim surface complicates the contact treatment further. In view of this, a local contact approach would be a better way to take care of the contacts instead of a global single surface contact approach. There are various possible combinations of local contacts that can be defined, but the tyre and tube should always be isolated for dedicated contact to facilitate troubleshooting. The general contact definitions employed in the present modelling, as listed in Table 3, have been found to improve the contact stability significantly.

However, there were several difficulties to be resolved before achieving the final complete run. Firstly it was found that the elements of the tube in the impact region experienced excessive fictitious contact oscillations as the striker started to press hard the tyre and tube against the rim. To improve the behaviour, the viscous contact damping (VDC)

Table 3: Contact definitions used in the present modelling

Contact Type	Part(s) Involved	SOFT Option
SINGLE_SURFACE	Hub, hub cover, bushing and axle	SOFT = 0
SURFACE_ TO_SURFACE	Hub to spokes	SOFT = 0
SURFACE_ TO_SURFACE	Rim to spokes	SOFT = 0
NODE_ TO_SURFACE	Bead wire to tube	SOFT = 0
SINGLE _SURFACE	Tyre and tube	SOFT = 2
SURFACE_ TO_SURFACE	Tyre and tube to rim and spoke	SOFT = 2
SURFACE_ TO_SURFACE	Striker to tyre	SOFT = 2

parameter on card 2 of the keyword *CONTACT was set to the critical damping value, i.e. 100%. But, at one stage when the rim and spokes had undergone significant plastic deformation it was again terminated, the elements of the tube at the impact region began to oscillate rigorously and then abruptly slipped away from the tyre into the area between the flanges of the rim, as depicted in Fig. 8a. It was rather obscure that such slipping behaviour had implicated the simulation, until a demonstration as depicted in Fig. 9 was performed. It was clearly seen that once the tube was fully compressed under continuous hard pressing load, together with the pressurized air inside and the significant friction between the tyre and tube, it remained in the same configuration without any slip. The instability was overcome by providing certain value to the mass weighted damping factor, MWD, in the *AIRBAG and for the most effective damping, a critical damping value was set. The tube then deformed smoothly, as illustrated in Fig. 8b, the oscillations were successfully minimized and the slipping phenomenon was eliminated as well. The last instability was caused by highly distorted and warped elements of the tube model in the impact region as they get fully pressed against the nipples. The issue was resolved by discretizing the corresponding elements into triangular elements and finally the simulation was completely run.

Model Validation

As comprehensive time histories of the relevant experimental data such as forces and accelerations

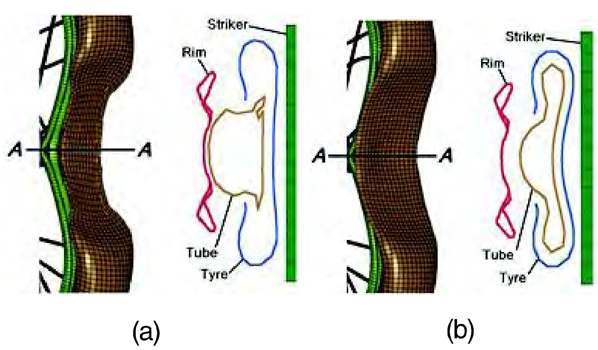

Fig. 8: (a) The behaviour of the tube following excessive oscillations. The right hand side shows the cross sectional A-A view cut at the vertex region of the V-shape deformed rim; (b) improved behaviour of the model upon adding a properly defined damping

Fig. 9: The cutaway view depicting the deflection profile and condition of the rim-tyre-tube assembly under full compression

were not available, some other quantifiable or measurable indicators needed to be defined for the validation purpose. The indicators that were selected are the overall deformation pattern of a wheel, the maximum residual crush (d) of a rim, the energy absorption of the wheel assembly (De), and the time histories of displacement and velocity of the striker. The overall deformation pattern of a wheel was selected as the first indicator, considering that the maximum residual crush of a rim and the velocity profile of a striker would be meaningless if even the general deformation is not comparable. The overall deformation pattern mainly compared the major characteristics of the bending of the rim and the buckling of the spokes throughout the impact process. However, for the light impacts which yielded relatively small bending of the rim but without any spoke buckling, it is reasonable to expect that it can well be taken care by just measuring the d. The instantaneous time history data of the displacement and velocity were not directly available due to lack of sensors, but were extracted from the video clips of a high speed camera capturing at 500 frame-per-seconds.

Results and Discussion

The *spg* configuration which yielded the second highest maximum residual crush was the one chosen for the initial modelling work. The overall deformations of the wheel at three different states in the simulation are presented in Fig. 10, together with its physical counterpart. The first frame shown is the midway between the striker just about to contact the tyre and the maximum engagement, the second is at the maximum engagement, while the third is the midway between the maximum engagement and the striker just leaving the tyre surface.

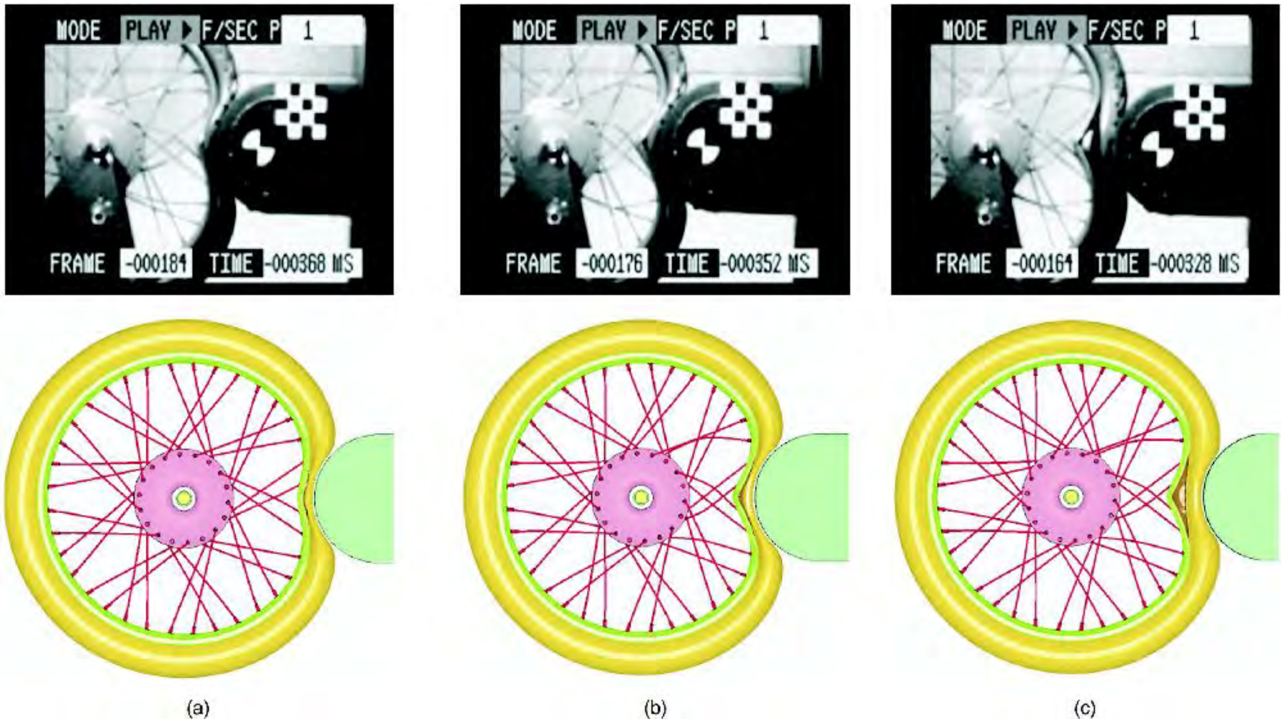

Fig. 10: Comparison of the overall deformation pattern of the wheel under the *spg* impact configurations at three different states of striker motion

The results showed some unmatched behaviours, particularly with regards to the buckling of the spoke, as highlighted in the Fig. 10b, which bent far lesser and in an opposite direction compared to the one in the experiment. From the examination, it was found that the nipple of the bent spokes were clamped and stuck at the holes. It was then understood that as the rim bent, the corresponding holes at the bent region tended to deform into oval shape, which would then clamp the spoke if the deformation is sufficiently severe. The unmatched behaviour could be due to the simplification done on the surface of the rim, as discussed in the previous section, *Rim*, see Fig. 5. Compared to the hole that is punched on the general surface, the one on the dented surface would be easier for the spoke to get stuck in the deformed hole as the dented surface provides a seat for the nipple. So it was speculated that slightly reducing the hole size could improve the result.

The average diameter size of the physical hole is 6.4 mm. With the contact thickness taken into consideration, the geometry of the rim has to be offset by half the thickness of the shell element. Since the thickness of the rim is 1.4 mm, the diameter of the hole of the rim model is given by 6.4 + 2(0.7) = 7.8 mm. To investigate the effects that could have on the interaction of rim-spoke due to the reduction of the size of the holes, two different diameter values were attempted, 7.6 and 7.7 mm. However, the 7.6 mm hole tended to cause significant initial penetration problem as the gap between the surface of the nipple and the edge of a hole is very small and impractical to adjust the nipple to the perfect centre. The 7.7 mm diameter has no such difficulties and was then successfully simulated.

The behaviour of the wheel assembly with updated rim is presented again in Fig. 11, together with its physical counterpart for comparison. Clearly seen, the results have been improved and the overall deformation patterns in the simulations closely matched the experimental one. It is interesting to note that the localized expansion, or the bulging, of the tube was successfully simulated as well, as highlighted in Fig. 11c. The δ, rounded to the nearest 1 mm, is close to the experimental value, i.e. 67 mm.

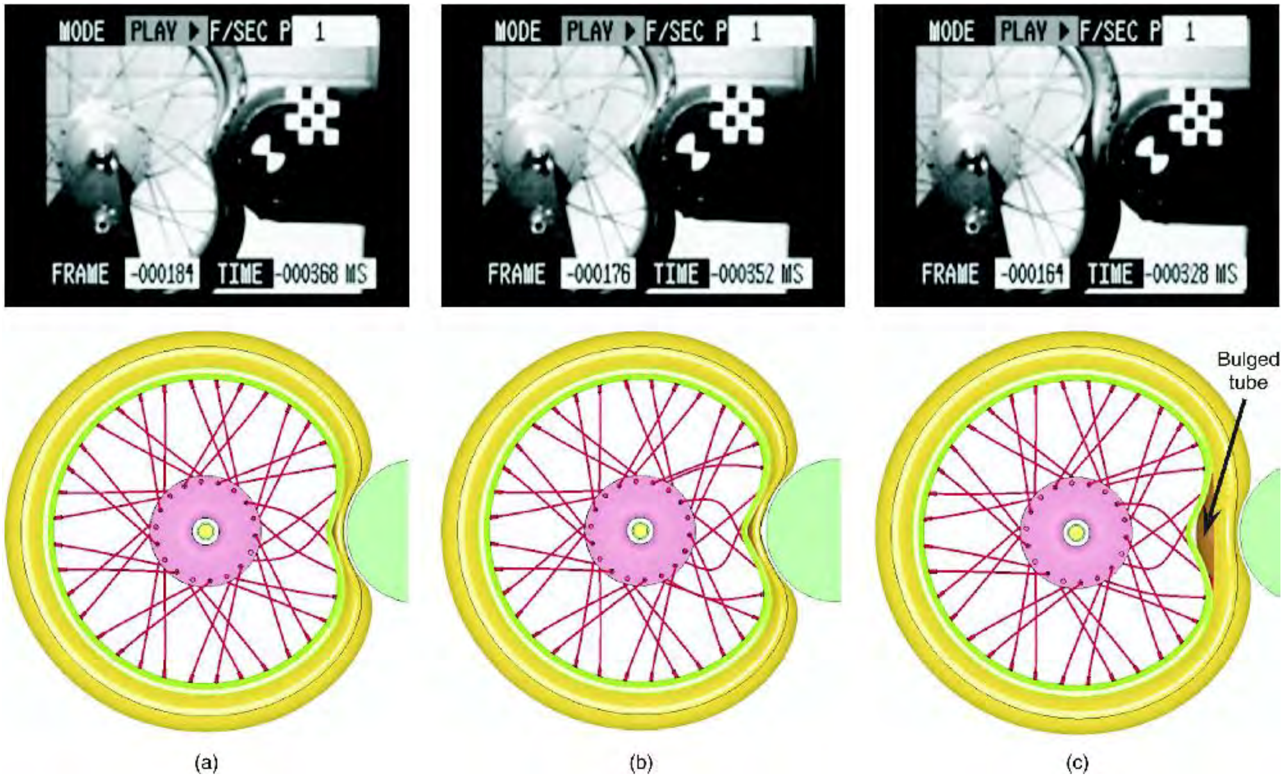

Fig. 11: Comparison of the overall deformation of the wheel for the *spg* configuration

The comparison of the time histories of the horizontal displacement and velocity of the striker for the *spg* configuration is presented in Fig. 12, showing that the time histories of the displacement and velocity of the striker in the simulation is reasonably consistent with the experimental one. Some deviations could be attributed to the frictional effect and the lateral vibration of the pendulum (twisting about the longitudinal axis of the pendulum) during the impact. The lateral vibration of the striker was observed from high speed camera clips. But in the simulations such effect is not taken into consideration as only the striker alone is incorporated and thus it is reasonable to expect the striker to have higher velocity of separation.

To quantify the deviations, the mean errors (ME), mean absolute error (MAE) and root mean square error (RMSE) were calculated and presented in Table 4. The simulations were then repeated for the other impact configurations, namely *s*, *m*, *p*, *g* and *mpg*. For the *s*, *m* and *mpg* configurations which are relatively moderate levels of impact, the overall deformations at three different states are depicted as in Fig. 13. But for the configurations *p* and *g* having a relatively light impact, there is no significant overall deformation observed and therefore no illustration is presented. The respective values of ME, MAE and RMSE for these configurations were computed and presented in Table 4 as well. The values of δ and Δε for the simulations are tabulated in Table 5 along with

Table 4: Calculated ME, MAE and RMSE for the time histories of displacement and velocity

Impact	Displacement			Velocity		
	ME	MAE	RMSE	ME	MAE	RMSE
spg	-5.75	6.79	8.51	-0.23	0.28	0.35
s	-5.13	7.38	9.56	-0.17	0.27	0.31
m	-5.84	6.27	8.32	-0.11	0.15	0.18
mpg	-4.09	4.09	4.95	-0.07	0.11	0.15
p	9.83	9.83	13.57	0.42	0.42	0.50
g	4.81	4.83	6.75	0.22	0.23	0.28

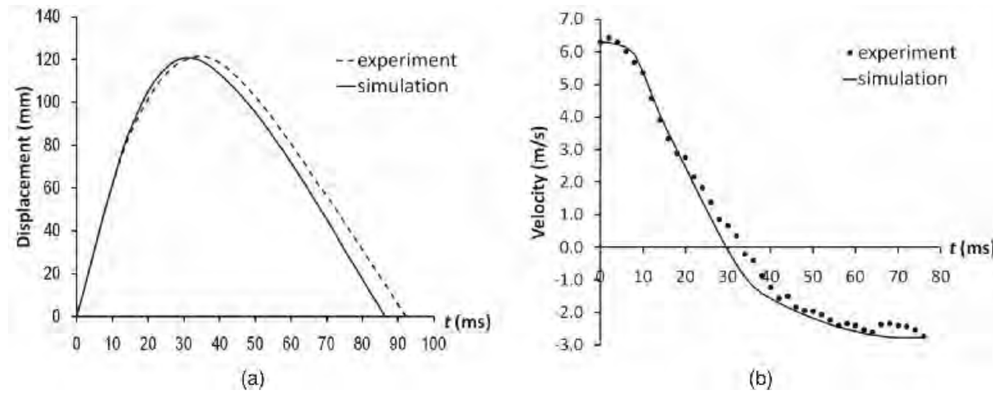

Fig. 12: Time histories of the (a) horizontal displacement and (b) velocity of the striker for the *spg* configuration

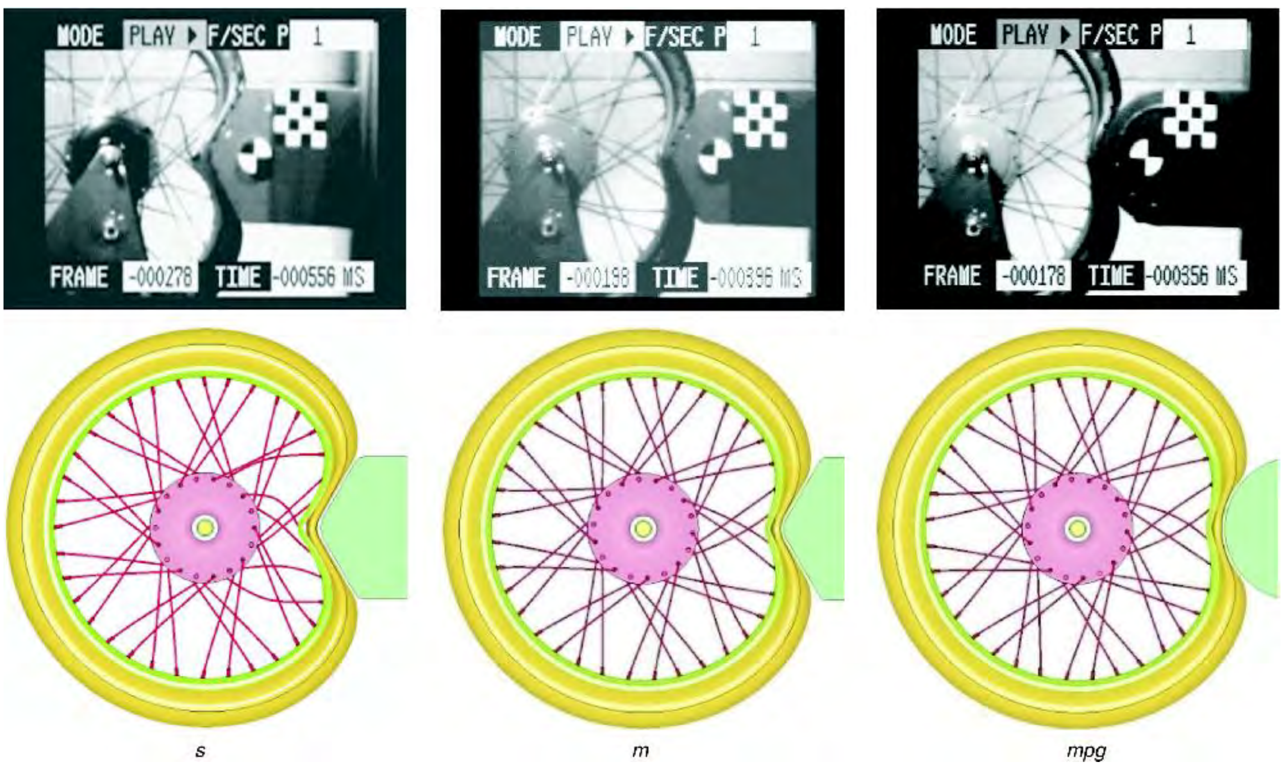

Fig. 13: Comparison of the overall deformation of the wheel under different impact configurations

the experimental results. The corresponding values of δ and Δε can be estimated from the empirical model as given by Equation (1) [23] and Equation (2) [24]. The notations are in accordance with Table 1.

$$\sqrt{\delta} = -0.219 + 0.0660\boldsymbol{S} + 0.00253\boldsymbol{M} - 0.0003\boldsymbol{P} - 0.000061\boldsymbol{SM} + 0.000039\boldsymbol{SP} + 0.0286\boldsymbol{SD} - 0.00456\boldsymbol{MD} + 2.15\boldsymbol{GD} \quad (1)$$

$$\sqrt{\Delta E} = -4.53 + 0.949\boldsymbol{S} + 0.0204\boldsymbol{M} - 0.00624\boldsymbol{P} - 0.120\boldsymbol{D} + 0.0110\boldsymbol{SM} + 0.00585\boldsymbol{SD} \quad (2)$$

To summarize, comparison of the results indicate that in general the present modelling work has successfully reproduced the corresponding experimental tests despite some discrepancies. The first discrepancy in the overall deformation is found in the *s* configuration, whereby the behaviour of all the spokes are reasonably matched with the experimental, except for the buckled spoke in the middle which has not bent to the extent as in the

Table 5: Comparison of the experimental and simulation results

No	Impact type	Maximum residual crush, δ (mm)		Energy absorbed, ΔE (J)	
		Experi-mental	Simu-lation	Experi-mental	Simu-lation
1	*spg*	67	67	760	660
2	*s*	81	79	810	690
3	*m*	40	41	360	430
4	*mpg*	29	32	330	370
5	*p*	4	9	130	90
6	*g*	4	9	140	100

experiment. The deviations in terms of ME, MAE and RMSE for all the configurations are basically the same as in the *spg* configuration, except for the *p* configurations. The largest deviation was found for the *p* and *g* configurations with respect to the δ and ΔE.

As discussed previously for the *spg* configuration, such discrepancy is again due to the simplification of the rim surface, i.e. the hole without the dented seat for the nipple. The nipple is therefore slid easily through the hole whenever the rim is bent and resisted only by the inflated tube. Upon the return of the striker after the maximum engagement, the spoke is progressively relaxed back. On the contrary, for the physical wheel with the nipple properly seated on the dented surface, the nipple easily gets stuck in the hole and was withheld till the end of the impact.

For the same reason, the deviation is also observed in δ for the *p* and *g* configurations. Physically, as the wheel deformed, the spokes were fully intact with the rim. But in the simulation, the rim departs from the spokes immediately as it deforms under the compression. The deformation of the rim is thus not fully resisted by the neighbouring spokes. Indeed, such behaviour also occurred in moderate and high intensity of impact configurations for certain wheel orientation. When the bending of the rim is sufficiently large, then to some extent the rim will depart from the spoke nipple. For those cases, the discrepancy in terms of the δ between the experimental and simulation tended to be relatively small as such behaviour had already been accounted for in the final permanent deformation. This is to be considered as the inherent characteristics of the present FE model of the complete wire-spoke motorcycle wheel. The further detailing of the dented spoke holes on the rim surface could be able to improve the results, but that would only significant for the light impact cases. Considering the ultimate application of the present model, i.e., to be installed on motorcycle model for full crash simulation in which often involves high impact energy, the simplified representation of the rim without the dented surface is adequate to serve the purpose.

Conclusion

1. A detailed model of a complete motorcycle wire-spoke wheel-tyre assembly was developed. The model has been validated against experimental results in terms of the overall deformation pattern, time histories of displacement and velocity, and maximum residual crush of the rim. The simulation results are comparable and consistent with the experimental results.

2. Parameters related to contact treatment that must be handled carefully in developing a stable and robust simulation model for the impact of the wire-spoke wheel-tyre assembly have been identified and discussed.

3. With fully deformable capability, the model can be used for parametric studies and also full motorcycle crash simulations under various configurations other than the frontal direct impact.

References

1. Ramet M, Cesari D and Dedoyaw A *6th IRCOBI Conf Biomechanics of Impacts* (1981) 193-205

2. Sporner A, Polauke J and Langwieder K *SAE Int Congress and Exposition* (1990) 197-206

3. Fujii S *JSAE Review* **24** (2003) 471-475

4. Chinn B P, Happian-Smith J and Macaulay M A *Int J Impact Eng* **8(3)** (1989) 265-273
5. Kanbe S, Deguchi M and Hannya Y *20th ESV* Paper No 07-0095 (2007)
6. Chawla A, Mukherjee S, Mohan D, Singh M, Sakurai M and Nakatani T *JARI Research J* **23(2)** (2001) 18-21
7. Chawla A, Mukherjee S, Mohan D, Bose D, Rawat P, Sakurai M and Nakatani T *18th ESV* Nagoya Japan (2003)
8. Mukherjee S, Chawla A, Mohan D and Singh M *IRCOBI Proc* (2001) 133-141
9. Nakatani T, Sakurai M, Chawla A and Mukherjee S *JSAE* 20015417 (2001)
10. Takatori O *JSAE Proc* **10(99)** (1999) 17-20
11. Namiki H, Nakamura T and Iijima S *SAE* 2003-32-0044 (2003)
12. Namiki H, Nakamura T and Iijima S *19th ESV* Paper No. 05-0309 (2005)
13. Watanabe Y and Kaldjian M J *Computer and Structures* **5-6(17)** (1983) 653-658
14. Daniele Barbani, Marco Pierini, Niccolo Baldanzini *Int J Crashworthines* **17(3)** (2012) 309-318
15. Tan K S, Wong S V, Radin Umar R S, Hamouda A M S and Gupta N K *Int J Impact Eng* **32(10)** (2006) 1554-1572
16. LSTC 2007. *LS-DYNA Keyword User's Manual*, Version 9.71, Livermore Software Technology Corporation, US
17. Tan K S, Wong S V, Seow M W, Radin Umar R S and S Hamouda A M *14th ISME Int Conf on Mechanical Engineering in Knowledge Age* (2005) 154-160
18. International Organization for Standardization, ISO 4249-3: 2010 - Motorcycle tyres and rims (code-designated series), Part 3: Rims, ISO, Geneva (2010)
19. Japanese Standard Association, 2009. JIS G3411: 2009 Cold-reduced carbon steel sheet and strip, JSA, Tokyo (2009)
20. Huh H, Lim J H and Park S H *Int J Automot Techn* **10(2)** (2009) 195-204
21. Belytschko T, Schwer L and Klein M J *Int J Numerical and Analytical Methods in Eng* **11(1)** (1977) 65-84
22. NADCA, NADCA Product Specification Standards for Die Castings, North American Die Casting Association (2006)
23. Tan K S, Wong S V, Radin Umar R S, Hamouda A M S and Gupta N K *Int J Automot Techn* **10** [3] (2009) 329-339.
24. Tan K S, Wong S V, Radin Umar R S, Hamouda A M S and Megat M M H Ahmad *Int J Crashworthines* **11(2)** (2006) 131-142.